RESEARCH ARTICLE

Carbon Recovery, Characterization, and Kinetic Modeling for Hydrogen Production and Phenol Adsorption

Taniya Rose Abraham[1,*], **Davis Johny**[2], **Kumar Anurag**[2], **Mary Varughese**[3] and **Sabu Thomas**[2]

[1] School of Energy Materials, Mahatma Gandhi University, Kottayam 686560, India
[2] Centre for High Performance Computing, Mahatma Gandhi University, Kottayam 686560, India
[3] Post-Graduate Department of Physics, St. Stephen's College, Pathanapuram 689695, India

Abstract

Catalytic methane decomposition (CMD) produces CO_x-free hydrogen together with solid carbon, but the carbon that accumulates on the catalyst is usually discarded with the spent material. Here, carbon deposited on a spent 30Ni-5Cu/activated-carbon (30Ni-5Cu/AC) CMD catalyst was recovered by nitric acid leaching as a functional carbon material and assessed as an adsorbent for phenol, with reuse as a catalyst support proposed. Leaching was carried out with 4–14 M HNO_3 at 75–105 °C, and the products were characterized by X-ray diffraction (XRD), N_2 physisorption, Fourier-transform infrared spectroscopy, and field-emission scanning electron microscopy. Treatment with 4 M HNO_3 at 90 °C or above removed the Ni and Ni-Cu phases while the graphitic (002) reflection at $2\theta \approx 26.4°$ was retained. Stronger acid fragmented the filamentous carbon. After functionalization with sodium thiosulfate, the recovered carbon (MLC-S) had a BET surface area of 1052 $m^2\,g^{-1}$. Phenol uptake on MLC-S at 30–70 °C followed the Langmuir model ($R^2 \geq 0.995$) and was higher than that on thiosulfate-treated commercial activated carbon (VAC-S) at every temperature. Uptake fell as temperature increased, which is consistent with exothermic adsorption. A Langmuir-Hinshelwood rate expression with first-order deactivation is proposed for the CMD step. These results show that carbon from spent CMD catalysts can be recovered and converted into a sustainable functional carbon material, linking hydrogen production with wastewater treatment.

Keywords: catalytic methane decomposition, hydrogen, spent catalyst, carbon recovery, acid leaching, phenol adsorption, Langmuir isotherm, sustainable functional carbon.

1 Introduction

World energy demand keeps rising with industrialization, urban growth and population, and fossil fuels still supply most of it. The resulting

Submitted: 15 September 2026
Revised: 08 October 2026
Accepted: 11 October 2026
Published: 24 November 2026

Vol. 2, **No.** 4, 2026.
10.62762/JAMR.2026.675203

***Corresponding author:**
✉ Taniya Rose Abraham
taniyakizhakkel@gmail.com

Citation
Abraham, T. R., Johny, D., Anurag, K., Varughese, M., & Thomas, S. (2026). Carbon Recovery, Characterization, and Kinetic Modeling for Hydrogen Production and Phenol Adsorption. *Journal of Advanced Materials Research*, 2(4), 313–322.

© 2026 by the Authors. Published by Institute of Central Computation and Knowledge. This is an open access article under the CC BY license (https://creativecommons.org/licenses/by/4.0/).

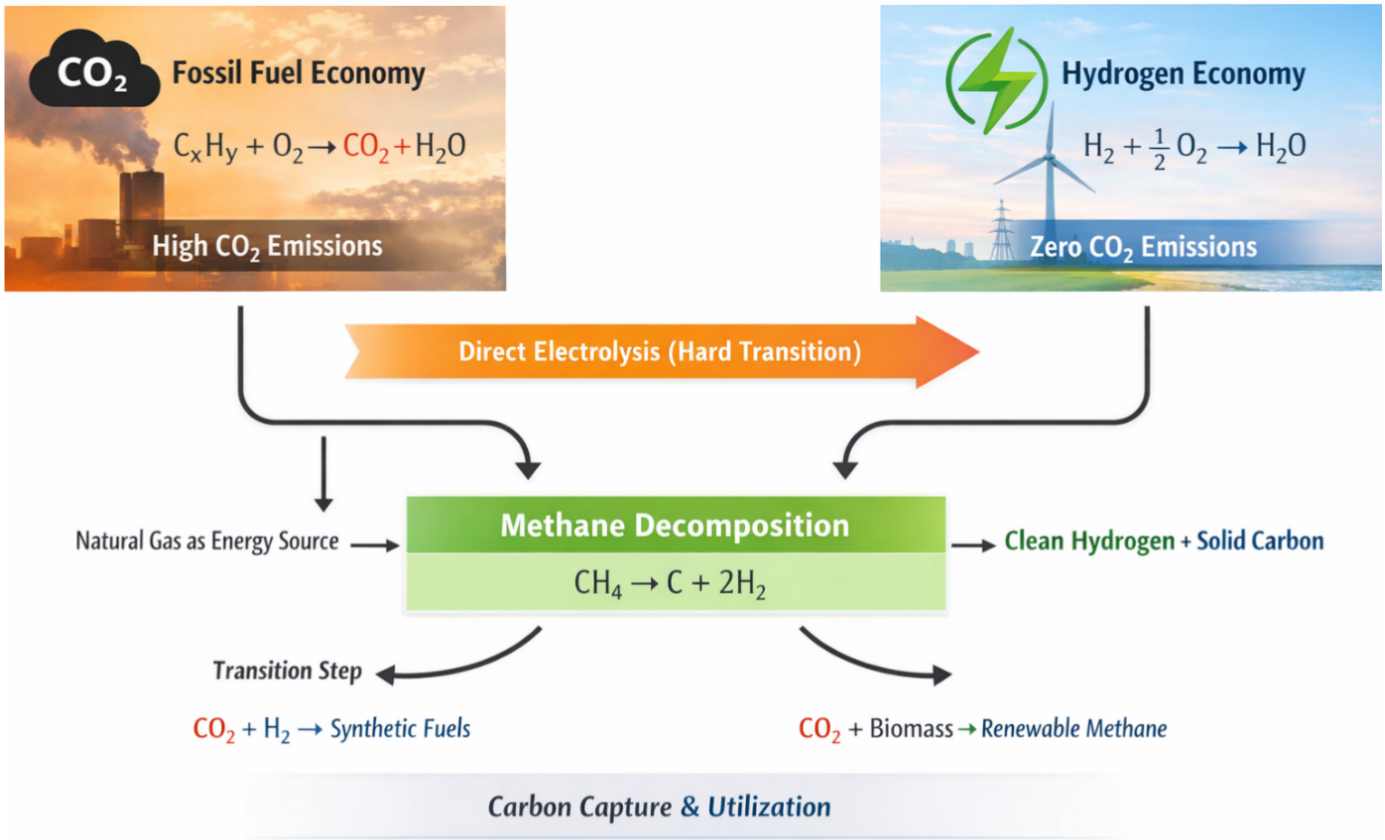

Figure 1. Conventional fossil-fuel-based hydrogen production compared with catalytic methane decomposition, which yields hydrogen and solid carbon with minimal direct CO_2 emission.

increase in atmospheric CO_2 is a main driver of climate change. The Paris Agreement and related assessments therefore call for deep decarbonization and a faster move to low-carbon energy [1–3]. Hydrogen is attractive in this setting because it has a high gravimetric energy density and emits no CO_2 at the point of use.

How clean hydrogen is depends on how it is made. Most industrial hydrogen comes from steam methane reforming (SMR), which is efficient but releases roughly 12 kg of CO_2-equivalent per kilogram of H_2 [4]. This has prompted work on routes with a smaller carbon footprint. One of them is direct methane decomposition, in which methane is split into hydrogen and solid carbon without forming CO or CO_2, either thermally [5] or over a catalyst (catalytic methane decomposition, CMD) [6]. CMD typically runs at 500–850 °C and yields both hydrogen and a carbon co-product (Figure 1).

Depending on catalyst composition and reaction conditions, the carbon co-product can be graphitic carbon, carbon nanotubes (CNTs) or carbon nanofibers (CNFs) [7]. The deposited carbon can also act as a catalyst for methane decomposition itself [8]. Carbon nanostructures of this kind have good mechanical, electrical and surface properties and are used in energy storage, catalysis and composites [9]. Selling the carbon can also improve the economics of CMD hydrogen relative to competing routes [10].

CMD has nevertheless seen little commercial use. The main obstacle is catalyst deactivation: carbon builds up on the active sites, reducing activity and shortening catalyst life [11]. Continuous reactor operation, separation of the deposited carbon and catalyst regeneration are also unresolved. Acid leaching is the usual way to strip metal particles and oxide supports from the carbon, but it can create structural defects, especially in CNTs, and degrade their properties [12, 13]. Physical separation based on magnetic, size or density differences is possible in principle but has received little experimental attention.

Water pollution is a parallel concern. Phenol is a priority pollutant released by the petrochemical, pharmaceutical, resin and coking industries. It is toxic, chemically stable and water-soluble, which makes it hard to remove by conventional treatment [14–16]. Adsorption is widely used because it is simple,

Table 1. Nomenclature and preparation conditions of the carbon samples used in this study.

Sample	Full name	Preparation route	Treatment conditions	Application
VAC	Virgin activated carbon	Commercial activated carbon used as reference material	Used without metal-leaching treatment	Reference adsorbent
VAC-S	Virgin activated carbon functionalized with sodium thiosulfate	VAC followed by sodium thiosulfate treatment	Aqueous $Na_2S_2O_3$ treatment $\rightarrow$ washing $\rightarrow$ drying	Phenol adsorption
MLC	Metal-leached carbon	Carbon recovered from spent 30Ni-5Cu/AC by acid leaching	4 M HNO_3 at 95 °C $\rightarrow$ filtration $\rightarrow$ washing to neutral pH $\rightarrow$ drying	Recovered carbon/precursor
MLC-S	Metal-leached carbon functionalized with sodium thiosulfate	MLC followed by sodium thiosulfate treatment	Aqueous $Na_2S_2O_3$ treatment $\rightarrow$ washing $\rightarrow$ drying	Phenol adsorption

effective and flexible [17]. Activated carbon is the most common adsorbent [18, 19], but its production is energy-intensive and depends on the choice of precursor, which motivates the search for alternative carbon sources, such as agricultural residues [20].

Carbon nanotubes and other nanostructured carbons, of the kind formed by methane decomposition, are promising adsorbents for phenolic compounds because of their aromatic surfaces, high surface area and modifiable surface chemistry [21, 22]. Multi-walled carbon nanotubes, for example, adsorb phenol and aniline from water effectively [23]. Surface chemistry strongly affects phenol uptake on carbons: oxidizing or sulfur-containing treatments introduce oxygen- and sulfur-bearing groups that change the surface polarity and the balance of hydrogen-bonding, π-π and electrostatic interactions with phenol [24].

Most CMD studies focus on catalyst design, hydrogen yield and nanocarbon synthesis, and few deal with what happens to the carbon afterwards. In particular, little is known about how to remove the metals without damaging the carbon structure, or how to adjust its surface chemistry for environmental use. In this work, carbon recovered from a spent activated-carbon-supported CMD catalyst is evaluated as an adsorbent for phenol in water, and its reuse as a catalyst support for CMD is proposed. We examine how acid-treatment conditions affect metal leaching, surface chemistry and adsorption, and compare the recovered carbon with commercial activated carbon.

2 Experimental Methodology

This section describes how carbon was recovered from spent CMD catalysts, functionalized and characterized, and how catalytic activity and phenol adsorption (isotherms, kinetics and thermodynamics) were evaluated.

2.1 Acid Leaching and Recovery of Carbon from Spent Catalyst

The spent catalyst, denoted 30Ni-5Cu/AC, was collected after CMD runs and contained deposited carbon together with residual nickel and copper on an activated-carbon support. Acid leaching was used to dissolve the metallic species while keeping the carbon formed during methane decomposition.

In a typical procedure, the spent catalyst was treated with nitric acid under defined conditions. The solid residue was then filtered off and washed repeatedly with deionized water until the washings were neutral, to remove residual acid and dissolved metal ions, and dried. The recovered carbon was used as an adsorbent for phenol and is proposed as a support for re-impregnation of active metals for CMD [25]. Sample names and preparation conditions are summarized in Table 1.

2.2 Surface Functionalization Using Sodium Thiosulfate

Before the adsorption tests, the recovered carbon was functionalized with sodium thiosulfate ($Na_2S_2O_3$) to introduce sulfur-containing groups, increase surface polarity and improve interaction with aromatic pollutants.

The acid-treated carbon was impregnated with aqueous $Na_2S_2O_3$, washed to remove excess precursor and dried. The functionalized samples were stored in airtight containers until use. Full details are given in the Supplementary Information.

2.3 Characterization of Catalysts and Carbon Materials

The crystalline structure and phase composition of fresh, spent and acid-treated catalysts were examined by X-ray diffraction (XRD; PANalytical Empyrean) at 45 kV and 40 mA with Cu Kα radiation ($\lambda = 1.5406$ Å). Patterns were recorded over $2\theta = 10$–80° with a step size of 0.04°, and phases were identified with the JCPDS database.

Specific surface area and pore characteristics were determined from N_2 adsorption-desorption isotherms measured at -196 °C on a Quantachrome Autosorb 6B analyzer after degassing at 200 °C for 3 h. The specific surface area was calculated by the Brunauer-Emmett-Teller (BET) method [26].

Surface functional groups were identified by Fourier-transform infrared spectroscopy (FT-IR; Nicolet 6700, USA) over 400–4000 cm^{-1}. Morphology of spent and acid-treated samples was examined by field-emission scanning electron microscopy (FE-SEM; JEOL JSM-7610F) after gold coating.

2.4 Evaluation of Catalytic Activity

CMD experiments were carried out in a quartz fixed-bed tubular reactor (internal diameter 10 mm, length 450 mm). A known amount of catalyst was placed at the center of the reactor and heated to the reaction temperature under inert gas, after which methane was introduced at a controlled flow rate.

Catalytic performance was evaluated from hydrogen production and catalyst stability. Products were analyzed online, and spent catalysts were collected for post-reaction characterization. Detailed conditions are given in the Supplementary Information.

2.5 Phenol Adsorption Experiments

Batch adsorption tests were performed with the $Na_2S_2O_3$-functionalized recovered carbon by contacting a known mass of adsorbent with phenol solutions of known concentration under controlled agitation. Samples were withdrawn at set times and analyzed for residual phenol.

The effects of contact time, initial phenol concentration and adsorbent dosage were studied, and the results were compared with those of commercial activated carbon. Procedures and analytical methods are described in the Supplementary Information.

2.6 Adsorption Isotherm Analysis

Equilibrium data were analyzed with the Langmuir, Freundlich and Temkin isotherms [27, 28]. The Langmuir isotherm is

$$q_e = \frac{q_{\max} K_L C_e}{1 + K_L C_e}, \tag{1}$$

the Freundlich isotherm is

$$q_e = K_F C_e^{1/n}, \tag{2}$$

and the Temkin isotherm is

$$q_e = \frac{RT}{b_T} \ln\left(K_T C_e\right). \tag{3}$$

Here q_e ($\mathrm{mg\,g^{-1}}$) is the amount adsorbed at equilibrium, C_e ($\mathrm{mg\,L^{-1}}$) the equilibrium phenol concentration, $q_{\max}$ ($\mathrm{mg\,g^{-1}}$) the Langmuir monolayer capacity, K_L ($\mathrm{L\,mg^{-1}}$) the Langmuir constant, K_F ($(\mathrm{mg\,g^{-1}})(\mathrm{L\,mg^{-1}})^{1/n}$) and n the Freundlich constants, b_T ($\mathrm{J\,mol^{-1}}$) and K_T ($\mathrm{L\,mg^{-1}}$) the Temkin constants, R (8.314 $\mathrm{J\,mol^{-1}\,K^{-1}}$) the gas constant and T (K) the absolute temperature.

2.7 Adsorption Kinetic Analysis

Adsorption kinetics were evaluated with the pseudo-first-order, pseudo-second-order [29] and intraparticle diffusion models [30]:

$$\ln\left(q_e - q_t\right) = \ln q_e - k_1 t, \tag{4}$$

$$\frac{t}{q_t} = \frac{1}{k_2 q_e^2} + \frac{t}{q_e}, \tag{5}$$

$$q_t = k_{id} t^{1/2} + C, \tag{6}$$

where q_t ($\mathrm{mg\,g^{-1}}$) is the amount adsorbed at time t (min), k_1 ($\mathrm{min^{-1}}$), k_2 ($\mathrm{g\,mg^{-1}\,min^{-1}}$) and k_{id} ($\mathrm{mg\,g^{-1}\,min^{-1/2}}$) are the rate constants of the three models, and C ($\mathrm{mg\,g^{-1}}$) is related to boundary-layer thickness.

2.8 Thermodynamic Analysis

Thermodynamic parameters were obtained from adsorption data at different temperatures [31]. The standard Gibbs free energy change was calculated from

$$\Delta G^\circ = -RT \ln K_c, \tag{7}$$

and the standard enthalpy (ΔH°) and entropy (ΔS°) changes from the van't Hoff equation:

$$\ln K_c = \frac{\Delta S^\circ}{R} - \frac{\Delta H^\circ}{RT}. \tag{8}$$

Here K_c is the dimensionless equilibrium constant.

2.9 Theoretical and Kinetic Modeling Framework

A semi-theoretical framework is used to link CMD kinetics, carbon structure and adsorption performance. CMD is treated as a surface-controlled catalytic process in which hydrogen production rate and catalyst stability depend on methane adsorption, surface reaction and carbon growth. The carbon formed during CMD is then used as an adsorbent, and its behavior is interpreted through measurable structural descriptors: BET surface area and pore volume represent the accessible surface and mesoporosity that control phenol diffusion and pore filling. Relating the CMD kinetic parameters and adsorption constants to these descriptors gives a structure-property-performance description of both catalytic activity and adsorption.

2.10 Mechanistic Kinetic Modeling of Catalytic Methane Decomposition

CMD kinetics are interpreted with a Langmuir-Hinshelwood-type mechanism in which methane adsorbs on active metal sites before surface C-H bond dissociation. The overall methane decomposition rate is

$$r_{CH_4} = \frac{k\, K_{CH_4}\, P_{CH_4}}{1 + K_{CH_4} P_{CH_4}}, \tag{9}$$

where k is the intrinsic surface rate constant, K_{CH_4} the methane adsorption equilibrium constant and P_{CH_4} the methane partial pressure. Deactivation caused by carbon accumulation on active sites is described by an exponential decay term:

$$r(t) = r_0 \exp(-\alpha t), \tag{10}$$

where r_0 is the initial reaction rate and α is the carbon-induced deactivation coefficient. Methane adsorption and C-H bond dissociation produce hydrogen and deposit carbon on the catalyst. Excess carbon can block active sites, but partial graphitization of the deposit keeps part of the surface accessible and prevents complete deactivation. This suggests that controlled carbon growth is important for balancing activity and stability.

3 Results and Discussion

3.1 Physicochemical Characterization of Acid-Treated Samples

The effect of nitric acid treatment on the structure of the spent 30Ni-5Cu/AC catalyst was examined by XRD as a function of acid concentration and treatment temperature. Figure 2(a) shows the patterns of the untreated spent catalyst and of samples treated with 4–14 M HNO_3 at 95 °C, and Figure 2(b) shows the effect of treatment temperature (75–105 °C) at a fixed HNO_3 concentration of 4 M.

The untreated spent catalyst shows diffraction peaks at $2\theta \approx 44.3°$, $52.1°$ and $76.0°$, assigned to metallic Ni and Ni-Cu alloy phases, which shows that metal species remain after CMD. A distinct peak at about $26.4°$, corresponding to the (002) plane of graphitic carbon, confirms that ordered carbon formed during the reaction.

After acid treatment, the metallic peaks become much weaker. Raising the HNO_3 concentration above 4 M does not reduce the Ni and Ni-Cu reflections much further, which indicates that most of the metal dissolves already at the lower concentration. On this basis, 4 M HNO_3 was selected for metal removal.

The effect of temperature was examined with 4 M HNO_3 (Figure 2(b)). At 75 °C, weak metallic peaks remain, suggesting incomplete leaching. Samples treated at 90 and 105 °C show almost no metallic peaks.

Both acid concentration and temperature therefore affect metal removal. A moderate HNO_3 concentration is enough for leaching, but a temperature of 90 °C or higher is needed to remove the metallic phases detectable by XRD. Under these conditions the carbon framework is retained.

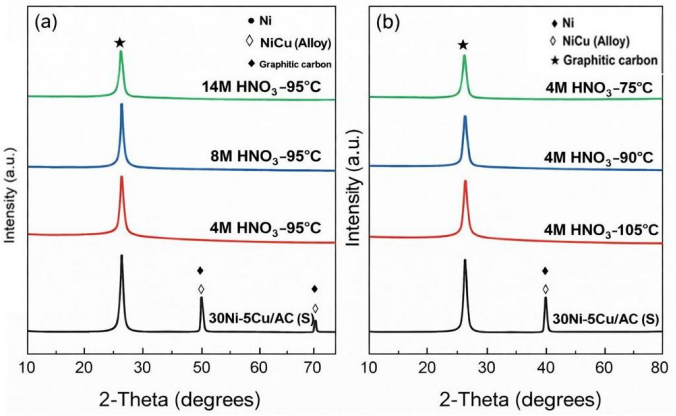

Figure 2. XRD patterns of the spent 30Ni-5Cu/AC catalyst before and after nitric acid treatment: (a) effect of HNO_3 concentration at 95 °C; (b) effect of treatment temperature with 4 M HNO_3.

3.2 Morphological Evolution of Acid-Treated Carbon

The SEM image of the untreated spent catalyst (Figure 3(a)) shows a surface densely covered

Table 2. BET surface area and pore characteristics of the spent catalyst and MLC-S.

Sample	S_{BET} ($m^2\,g^{-1}$)	V_{total} ($cm^3\,g^{-1}$)	V_{micro} ($cm^3\,g^{-1}$)	V_{meso} ($cm^3\,g^{-1}$)	D_{avg} (nm)
30Ni-5Cu/AC (S)	80.1	0.13	0.004	0.119	6.10
MLC-S	1052	0.56	0.226	0.338	2.30

by an interconnected network of filamentous carbon. At higher magnification (Figure 3(b)) the filaments are long, thin and highly entangled, with fairly uniform diameters, confirming that well-developed filamentous carbon formed during methane decomposition.

Based on the available data, the recovered carbon is best described as predominantly filamentous graphitic carbon rather than being assigned to either CNTs or CNFs. SEM shows long, thin, entangled filaments, and XRD shows the (002) graphitic reflection at $2\theta \approx 26.4°$, so the carbon is graphitic with a CNT/CNF-like filamentous morphology. Distinguishing CNTs from CNFs would require direct nanoscale imaging such as TEM.

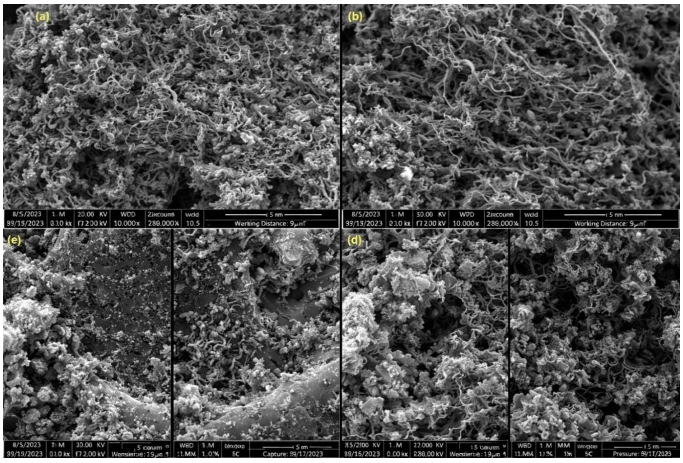

Figure 3. SEM images of (a, b) the spent 30Ni-5Cu/AC catalyst after CMD; (c, d) carbon recovered after treatment with 4 M HNO_3 at 95 °C; (e, f) carbon treated with 8 M HNO_3 at 95 °C; and (g, h) carbon treated with 14 M HNO_3 at 95 °C.

After treatment with 4 M HNO_3, the morphology changes noticeably (Figure 3(c, d)): the filaments are less densely packed and partly broken. This is attributed to partial oxidation of the carbon surface during the mild treatment at 95 °C.

With 8 M HNO_3 the surface changes markedly (Figure 3(e, f)). The carbon framework is strongly fragmented, with a porous, sponge-like texture and few continuous filaments left.

With 14 M HNO_3 (Figure 3(g, h)) the morphology is severely degraded. The fibrous network is largely destroyed and replaced by irregular, agglomerated fragments. This is attributed to aggressive oxidation by the concentrated acid.

Overall, nitric acid concentration and treatment temperature strongly influence the morphology and structural integrity of the carbon recovered from spent CMD catalysts. Moderate treatment removes the metals while keeping partly ordered carbon, whereas concentrated acid causes extensive oxidation and morphological damage.

3.3 Adsorption Isotherms and Structure-Property Correlation

Figure 4 shows the equilibrium isotherms of phenol on VAC-S and MLC-S at 30, 50 and 70 °C (303, 323 and 343 K). For both adsorbents, q_e increased with phenol concentration, indicating progressive occupation of adsorption sites. At every temperature MLC-S adsorbed more phenol than VAC-S (Table 3). Textural data are listed in Table 2.

The adsorption behavior can be related to the XRD results. The (002) reflection at $2\theta \approx 26.4°$ persists, showing that ordered graphitic domains are present; these domains favor phenol adsorption through π-π interactions between the aromatic ring and the graphitic surface [21]. The disappearance of the Ni and Ni-Cu reflections after acid treatment indicates that the metal phases fell below the XRD detection limit, leaving a cleaner carbon surface that is more accessible and free of competing metal sites.

Although VAC-S has a markedly lower BET surface area, it still adsorbs a large amount of phenol. This is attributed to its mesopore volume (0.305 $cm^3\,g^{-1}$), which is close to that of MLC-S (0.338 $cm^3\,g^{-1}$) and governs phenol access. Given the molecular size of phenol (about 0.6–0.9 nm), diffusion into the ultramicropores and narrow micropores that account for much of the surface area of VAC-S is sterically hindered. Adsorption is therefore controlled mainly by the mesopores and surface chemistry rather than by total surface area, which explains the similar trends despite the large difference in surface area.

At higher equilibrium concentrations the uptake tends toward a plateau for both materials, consistent with

Table 3. Langmuir and Freundlich isotherm parameters for phenol adsorption on MLC-S and VAC-S.

Model	Parameter	MLC-S			VAC-S		
		30 °C	50 °C	70 °C	30 °C	50 °C	70 °C
Langmuir	K_L (L mg^{-1})	0.0111	0.0067	0.0042	0.0136	0.0070	0.0043
	q_{max} (mg g^{-1})	3898.4	3456.2	3421.6	3538.7	3382.4	2652.9
	R^2	0.9980	0.9971	0.9953	0.9165	0.9898	0.8972
Freundlich	K_F[a]	342.8	160.3	129.6	142.5	104.6	66.1
	n	2.79	2.17	2.20	1.98	1.88	1.75
	R^2	0.9351	0.9768	0.9539	0.9294	0.8782	0.7921

[a] Unit of K_F: (mg g^{-1})(L mg^{-1})$^{1/n}$.

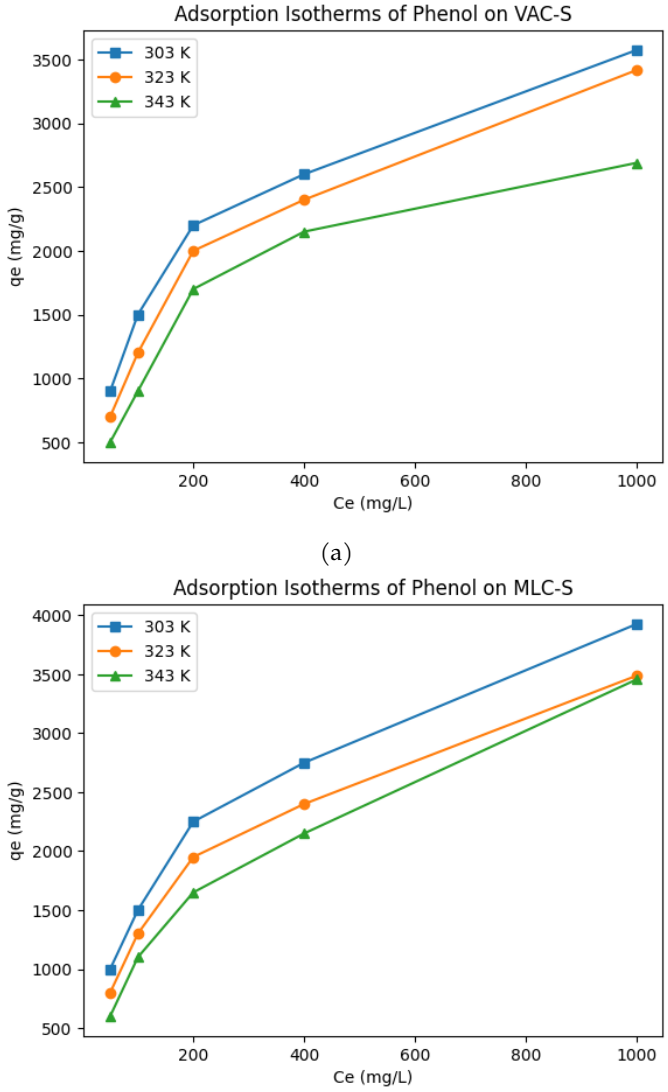

Figure 4. Adsorption isotherms of phenol on (a) VAC-S and (b) MLC-S at 30, 50 and 70 °C (303, 323 and 343 K).

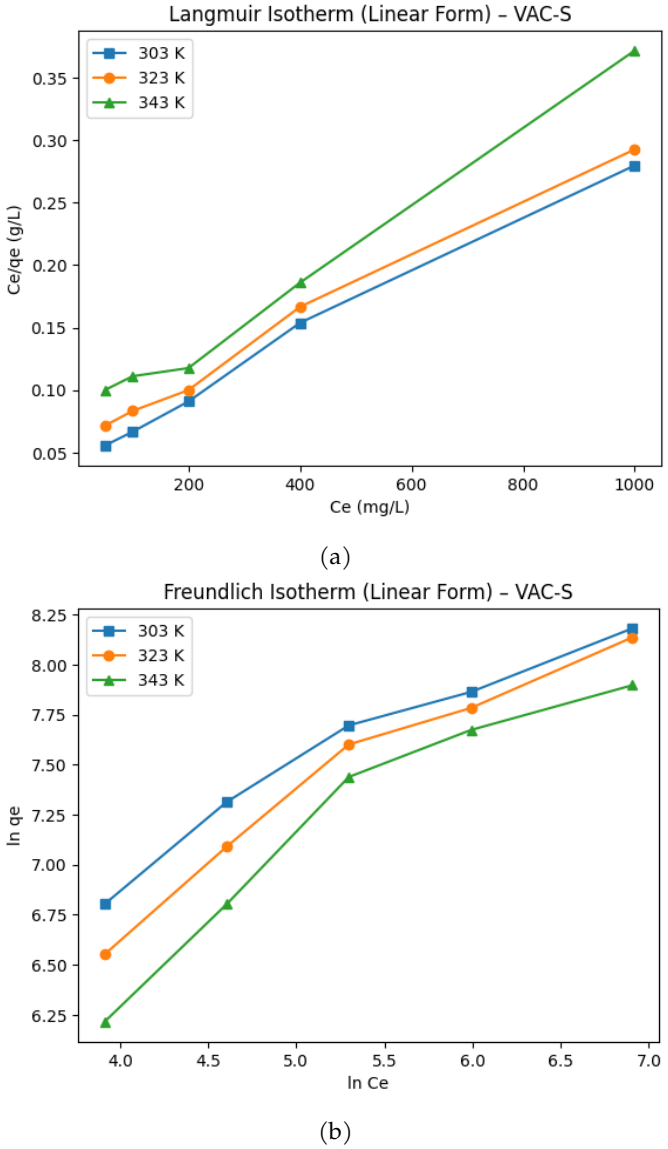

Figure 5. Linearized (a) Langmuir and (b) Freundlich plots for phenol adsorption on VAC-S at 30, 50 and 70 °C (303, 323 and 343 K).

saturation of the adsorption sites and monolayer adsorption. Adsorption capacity also decreased as temperature rose from 30 to 70 °C, which indicates that phenol adsorption is exothermic [30, 31].

The Langmuir and Freundlich models were fitted to

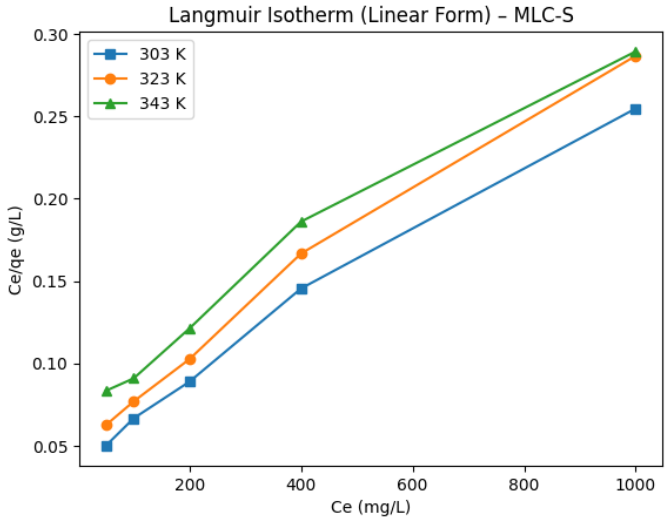

(a)

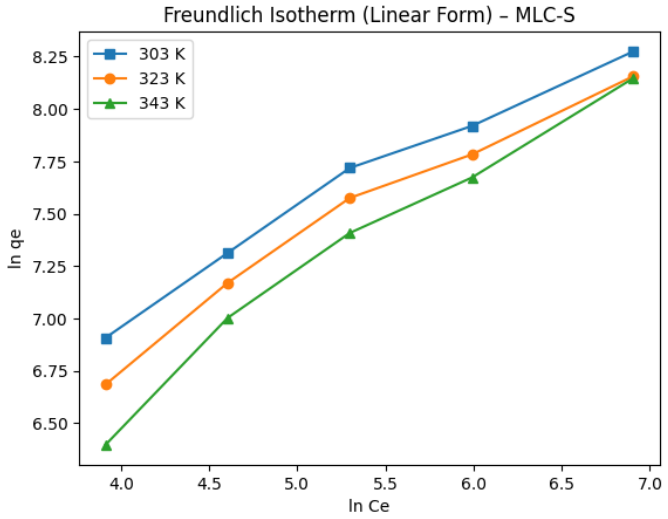

(b)

Figure 6. Linearized (a) Langmuir and (b) Freundlich fits for MLC-S at the same three temperatures.

the equilibrium data (Figures 5 and 6). For MLC-S the Langmuir model gave higher correlation coefficients than the Freundlich model at all temperatures ($R^2 = 0.9953$–0.9980; Table 3), suggesting monolayer adsorption on a fairly homogeneous surface. For VAC-S the Langmuir model fitted better at 50 and 70 °C, whereas at 30 °C the Freundlich model gave a slightly higher R^2 (0.9294 vs. 0.9165). The Langmuir capacity of MLC-S was 3898.4 mg g^{-1} at 30 °C and decreased to 3456.2 and 3421.6 mg g^{-1} at 50 and 70 °C, consistent with exothermic adsorption. The corresponding values for VAC-S were 3538.7, 3382.4 and 2652.9 mg g^{-1}. Freundlich n values above 1 for both adsorbents also indicate favorable adsorption.

The higher uptake of MLC-S can be attributed to the combination of retained graphitic order (the 26.4° reflection) and surface functionalization, which is expected to add oxygen- and sulfur-containing groups that modify the surface polarity and the hydrogen-bonding and electrostatic interactions with phenol. The net effect of such groups depends on their type and amount [24].

4 Conclusions

Carbon deposited on a spent 30Ni-5Cu/AC CMD catalyst was recovered by nitric acid leaching and reused as a phenol adsorbent, with reuse as a catalyst support proposed. The main findings are as follows.

1. CMD produced partly ordered filamentous graphitic carbon, identified by the XRD (002) reflection at $2\theta \approx 26.4°$ and by SEM. Treatment with 4 M HNO_3 at 90 °C or above removed the Ni and Ni-Cu phases without destroying the graphitic framework. Higher acid concentrations fragmented the filaments, so the leaching step has to balance metal removal against loss of carbon structure.

2. After thiosulfate functionalization, the recovered carbon (MLC-S, 1052 m^2 g^{-1}) adsorbed more phenol than functionalized commercial activated carbon (VAC-S) at 30, 50 and 70 °C. Uptake on MLC-S followed the Langmuir model ($R^2 \geq 0.995$) and decreased with temperature, which indicates exothermic adsorption and favors operation at lower temperature.

3. Retained graphitic domains (π-π interactions) and oxygen- and sulfur-containing surface groups (expected from the functionalization, but not verified by the data shown here) are likely to contribute to phenol binding, and accessible mesoporosity appears to matter more than total surface area.

Carbon formed during CMD, usually regarded as the cause of catalyst deactivation, can thus be converted into a useful adsorbent, linking hydrogen production with water treatment. Kinetic and thermodynamic parameters, CMD activity of the re-impregnated support, and multicycle adsorption tests are needed to confirm the practical value of this route.

Data Availability Statement

The data supporting the findings of this study are available within the article. Additional data are available from the corresponding author upon reasonable request.

Funding

This work was supported without any funding.

Conflicts of Interest

Taniya Rose Abraham and Sabu Thomas were members of the Editorial Board of *Journal of Advanced Materials Research* at the time of manuscript submission. To ensure the integrity and impartiality of the peer-review process, neither author was involved in the editorial handling, peer review, or decision-making for this manuscript, which was handled independently by another editor. The remaining authors declare no conflicts of interest.

AI Use Statement

The authors declare that no generative AI was used in the preparation of this manuscript.

Ethical Approval and Consent to Participate

Not applicable. This study did not involve human participants or animals.

References

[1] International Energy Agency. (2023). *World Energy Outlook 2023*. IEA, Paris. Retrieved from https://www.iea.org/reports/world-energy-outlook-2023

[2] IPCC. (2023). *Climate Change 2023: Synthesis Report*. Contribution of Working Groups I, II and III to the Sixth Assessment Report of the Intergovernmental Panel on Climate Change. IPCC, Geneva. [CrossRef]

[3] UNFCCC. (2015). *Paris Agreement*. United Nations Framework Convention on Climate Change, Bonn. Retrieved from https://unfccc.int/sites/default/files/resource/parisagreement_publication.pdf

[4] Spath, P. L., & Mann, M. K. (2001). *Life Cycle Assessment of Hydrogen Production via Natural Gas Steam Reforming* (Technical Report NREL/TP-570-27637). National Renewable Energy Laboratory, Golden, CO. Available online at: https://www.fischer-tropsch.org/DOE/DOE_reports/NREL/TP-570/TP-570-27637/TP-570-27637.pdf

[5] Abánades, A., Rubbia, C., & Salmieri, D. (2013). Thermal cracking of methane into hydrogen for a CO_2-free utilization of natural gas. *International Journal of Hydrogen Energy, 38*(20), 8491-8496. [CrossRef]

[6] Muradov, N. (2001). Hydrogen via methane decomposition: an application for decarbonization of fossil fuels. *International Journal of Hydrogen Energy, 26*(11), 1165-1175. [CrossRef]

[7] Snoeck, J.-W., Froment, G. F., & Fowles, M. (1997). Kinetic study of the carbon filament formation by methane cracking on a nickel catalyst. *Journal of Catalysis, 169*(1), 250-262. [CrossRef]

[8] Muradov, N., Smith, F., & T-Raissi, A. (2005). Catalytic activity of carbons for methane decomposition reaction. *Catalysis Today, 102-103*, 225-233. [CrossRef]

[9] Dresselhaus, M. S., Dresselhaus, G., & Avouris, Ph. (Eds.). (2001). *Carbon Nanotubes: Synthesis, Structure, Properties, and Applications* (Topics in Applied Physics, Vol. 80). Springer, Berlin. [CrossRef]

[10] Keipi, T., Tolvanen, H., & Konttinen, J. (2018). Economic analysis of hydrogen production by methane thermal decomposition: Comparison to competing technologies. *Energy Conversion and Management, 159*, 264-273. [CrossRef]

[11] Ashik, U. P. M., Daud, W. W., & Abbas, H. F. (2015). Production of greenhouse gas free hydrogen by thermocatalytic decomposition of methane–A review. *Renewable and Sustainable Energy Reviews, 44*, 221-256. [CrossRef]

[12] Datsyuk, V., Kalyva, M., Papagelis, K., Parthenios, J., Tasis, D., Siokou, A., Kallitsis, I., & Galiotis, C. (2008). Chemical oxidation of multiwalled carbon nanotubes. *Carbon, 46*(6), 833-840. [CrossRef]

[13] Chiang, Y. C., Lin, W. H., & Chang, Y. C. (2011). The influence of treatment duration on multi-walled carbon nanotubes functionalized by H_2SO_4/HNO_3 oxidation. *Applied Surface Science, 257*(6), 2401-2410. [CrossRef]

[14] Michałowicz, J., & Duda, W. (2007). Phenols - sources and toxicity. *Polish Journal of Environmental Studies, 16*(3), 347-362. https://www.pjoes.com/pdf-87995-21854

[15] Busca, G., Berardinelli, S., Resini, C., & Arrighi, L. (2008). Technologies for the removal of phenol from fluid streams: A short review of recent developments. *Journal of Hazardous Materials, 160*(2-3), 265-288. [CrossRef]

[16] Dąbrowski, A., Podkościelny, P., Hubicki, Z., & Barczak, M. (2005). Adsorption of phenolic compounds by activated carbon - a critical review. *Chemosphere, 58*(8), 1049-1070. [CrossRef]

[17] Ahmaruzzaman, M. (2008). Adsorption of phenolic compounds on low-cost adsorbents: A review. *Advances in Colloid and Interface Science, 143*(1-2), 48-67. [CrossRef]

[18] Marsh, H., & Rodríguez-Reinoso, F. (2006). *Activated Carbon*. Elsevier, Amsterdam. [CrossRef]

[19] Bansal, R. C., & Goyal, M. (2005). *Activated Carbon Adsorption*. CRC Press, Boca Raton, FL. https://api.taylorfrancis.com/content/books/mono/download?identifierName=doi&identifierValue=10.1201/9781420028812&type=googlepdf

[20] Ioannidou, O., & Zabaniotou, A. (2007). Agricultural residues as precursors for activated carbon production - A review. *Renewable and Sustainable Energy Reviews, 11*(9), 1966-2005. [CrossRef]

[21] Lin, D., & Xing, B. (2008). Adsorption of phenolic compounds by carbon nanotubes: Role of aromaticity and substitution of hydroxyl groups. *Environmental Science & Technology, 42*(19), 7254-7259. [CrossRef]

[22] Gupta, V. K., & Saleh, T. A. (2013). Sorption of pollutants by porous carbon, carbon nanotubes and fullerene-an overview. *Environmental Science and Pollution Research, 20*(5), 2828-2843. [CrossRef]

[23] Yang, K., Wu, W., Jing, Q., & Zhu, L. (2008). Aqueous adsorption of aniline, phenol, and their substitutes by multi-walled carbon nanotubes. *Environmental Science & Technology, 42*(21), 7931-7936. [CrossRef]

[24] Bandosz, T. J. (Ed.). (2006). *Activated Carbon Surfaces in Environmental Remediation* (Interface Science and Technology, Vol. 7). Elsevier, Amsterdam. https://www.sciencedirect.com/bookseries/interface-science-and-technology/vol/7/suppl/C

[25] Rodríguez-Reinoso, F. (1998). The role of carbon materials in heterogeneous catalysis. *Carbon, 36*(3), 159-175. [CrossRef]

[26] Thommes, M., Kaneko, K., Neimark, A. V., Olivier, J. P., Rodríguez-Reinoso, F., Rouquerol, J., & Sing, K. S. W. (2015). Physisorption of gases, with special reference to the evaluation of surface area and pore size distribution (IUPAC Technical Report). *Pure and Applied Chemistry, 87*(9-10), 1051-1069. [CrossRef]

[27] Ruthven, D. M. (1984). *Principles of Adsorption and Adsorption Processes*. Wiley, New York. https://www.wiley.com/en-us/shop/general-chemistry/principles-of-adsorption-and-adsorption-processes-p-9780471866060

[28] Foo, K. Y., & Hameed, B. H. (2010). Insights into the modeling of adsorption isotherm systems. *Chemical Engineering Journal, 156*(1), 2-10. [CrossRef]

[29] Ho, Y. S., & McKay, G. (1999). Pseudo-second order model for sorption processes. *Process Biochemistry, 34*(5), 451-465. [CrossRef]

[30] Liu, Q.-S., Zheng, T., Wang, P., Jiang, J.-P., & Li, N. (2010). Adsorption isotherm, kinetic and mechanism studies of some substituted phenols on activated carbon fibers. *Chemical Engineering Journal, 157*(2-3), 348-356. [CrossRef]

[31] Patil, P., Jeppu, G., Vallabha, M. S., & Girish, C. R. (2024). Enhanced adsorption of phenolic compounds using biomass-derived high surface area activated carbon: Isotherms, kinetics and thermodynamics. *Environmental Science and Pollution Research, 31*(60), 67442-67460. [CrossRef]

Taniya Rose Abraham is an Assistant Professor at the School of Energy Materials, Mahatma Gandhi University, Kottayam, Kerala, India. She holds an Integrated M.Sc.-Ph.D. in Chemistry (Chemical Physics). Her research interests include theoretical and computational chemistry, simulation of polymer chains in dilute solution, and atomistic modeling of energy materials using machine learning. (Email: corresponding-author@email.com)

Davis Johny is an Assistant Professor at the School of Energy Materials, Mahatma Gandhi University, Kottayam, Kerala, India. He holds an M.Sc. in Electronics and has qualified the National Eligibility Test (NET). His research interests include renewable energy, power electronics and thin-film perovskite solar cells.

Kumar Anurag is with the School of Energy Materials, Mahatma Gandhi University, Kottayam, Kerala, India. He holds an Integrated M.Tech. in Nanotechnology and has submitted his Ph.D. dissertation in Nanoscience and Nanotechnology. His research interests include two-dimensional materials such as graphene, graphene oxide, reduced graphene oxide and MoS_2 for energy applications, thin films, II-VI semiconductors and soft magnetic materials.

Mary Varughese is an Assistant Professor in the Post-Graduate Department of Physics, St. Stephen's College, Pathanapuram, Kerala, India. She holds M.Sc. and M.Phil. degrees in Physics, a Ph.D. from Mahatma Gandhi University and an MCA from IGNOU. Her research interests include experimental and theoretical studies of biomolecules and their interactions, crystallography and related computation, and nanomaterials for energy.

Sabu Thomas is a Professor at Mahatma Gandhi University, Kottayam, Kerala, India, and Director of the School of Energy Materials and of the International and Inter-University Centre for Nanoscience and Nanotechnology. His research covers polymer science and engineering, polymer nanocomposites, elastomers, polymer blends, membranes, green composites, nanomedicine, green nanotechnology and energy storage. He received his Ph.D. in Engineering from IIT Kharagpur and is a Fellow of the Royal Society of Chemistry (FRSC) and of the European Academy of Sciences (FEurASc).